High-Throughput Nonlinear Optical Microscopy

Peter T. C. So,[†‡§¶*] Elijah Y. S. Yew,[¶] and Christopher Rowlands[‡§]
[†]Department of Mechanical Engineering, [‡]Department of Biological Engineering, and [§]Laser Biomedical Research Center, Massachusetts Institute of Technology, Cambridge, Massachusetts; and [¶]BioSyM Interdisciplinary Research Group, Singapore-MIT Alliance for Research and Technology, Singapore, Singapore

ABSTRACT High-resolution microscopy methods based on different nonlinear optical (NLO) contrast mechanisms are finding numerous applications in biology and medicine. While the basic implementations of these microscopy methods are relatively mature, an important direction of continuing technological innovation lies in improving the throughput of these systems. Throughput improvement is expected to be important for studying fast kinetic processes, for enabling clinical diagnosis and treatment, and for extending the field of image informatics. This review will provide an overview of the fundamental limitations on NLO microscopy throughput. We will further cover several important classes of high-throughput NLO microscope designs with discussions on their strengths and weaknesses and their key biomedical applications. Finally, this review will close with a perspective of potential future technological improvements in this field.

INTRODUCTION

Nonlinear optical (NLO) microscopy covers a broad spectrum of high-resolution imaging modalities using contrast generated by the interaction between molecules and ultrafast light pulses. The two-photon absorption process was first predicted by Göppert-Mayer in 1931 (1) and was later developed by Sheppard et al. (2) and Denk et al. (3) into a powerful microscopic imaging technique for biology and medicine.

NLO microscopy has a number of important strengths:

First, NLO microscopy has inherent depth discrimination based on the quadratic and higher-order dependence of signal on the excitation photon flux distribution, which allows straightforward three-dimensional imaging. Importantly, the depth discrimination of NLO microscopy originates from the excitation process, permitting deeper imaging into turbid specimens; this is unlike confocal microscopy, which requires the presence of a physical pinhole aperture in the detection path, resulting in many of the scattered signal photons being lost.

Second, NLO excitation wavelengths typically lie in the infrared region, resulting in significantly lower tissue scattering and absorption, thereby further increasing imaging depth.

Third, photodamage and photobleaching are reduced and localized to the excitation volume, further enabling in vivo applications.

Fouth, spectroscopically resolved imaging, based on the different NLO modalities, enables monitoring of specimen biophysical and biochemical states by quantifying the geometry, the vibronic and electronic states, and the aggregation of probe molecules. Today, the most broadly used modality is based on two-photon excited fluorescence; however, newer modalities such as harmonic generation and nonlinear Raman processes are rapidly gaining ground.

The basic concept of NLO microscopy and its different variants have been thoroughly reviewed previously (4–6). This review takes a narrow focus on recent instrumental advances that enhance the throughput of NLO microscopy and some emergent biomedical applications.

The development of high-throughput NLO microscopy is driven by three types of biomedical applications:

First, many interesting biological processes occur in milliseconds and are thus inherently fast. Quantitative understanding of these processes often requires imaging these kinetic events within the three-dimensional structural constraints of the underlying cells and tissues. Examples include the electrical processes such as action potential propagation in myocytes (7), chemical processes such as second messenger propagation in neurons (8), and mechanical processes such as the contraction of cardiac tissues (9).

Second, NLO microscopy may be employed as a diagnostic tool in clinics. Although still at an early stage, international clinical trials are now underway in using NLO microscopy to diagnose a number of skin diseases such as melanoma (10,11). Preclinical studies are also underway to study processes such as liver fibrosis (12,13) and nerve remyelination (14,15). For clinical applications, imaging speed is critical in improving diagnostic accuracy by reducing motion effects that are physiological in origin and in decreasing treatment duration, which in turn alleviates patient discomfort and decreases medical cost.

Third, during the past decade, systems biology has emerged as a successful approach for understanding how complex protein-interaction pathways regulate many biological processes. Complex pathways are deciphered by

Submitted May 20, 2013, and accepted for publication August 22, 2013.

*Correspondence: ptso@mit.edu

Editor: Brian Salzberg.

0006-3495/13/12/2641/14 $2.00

http://dx.doi.org/10.1016/j.bpj.2013.08.051

monitoring cellular responses under many different perturbations, such as changing the level of protein expressions. In these studies, the large number of experiments requires the availability of high-throughput investigation tools. These tools included microarrays to profile gene and protein expression, mass spectroscopy to quantify protein modifications, and statistics, data mining, and modeling software for the analysis of these complex data. For the study of cellular processes involving significant morphological changes, imaging is emerging as an important new tool for system biology investigations. Pioneered by Perlman et al. (16,17) with a multivariate drug assay, imaging technology is a powerful tool as it not only provides morphological information, but can also simultaneously quantify the associated molecular, biochemical, and functional states of cells and tissues. Subsequently, this methodology has been applied to study pharmaceutical regulation of a variety of cellular functions such as migration (18), cytokinesis (19), nuclear export (20), mitotic spindle length determination (21), melanogenesis (22), aggresome formation (23), and membrane transport (24). It is expected that this method will be vital for pharmaceutical discovery in the future (25,26). Today, the field of image informatics is being extended to study processes in complex tissues and organs, and high-throughput, minimally invasive NLO microscopy imaging is expected to play an important role.

FUNDAMENTAL LIMITS ON NLO MICROSCOPY THROUGHPUT

An understanding of the factors limiting nonlinear microscopy throughput, and some common strategies to overcome them, will allow better appreciation of the relative strengths and weaknesses of the different implementations of high-throughput NLO microscopes covered in the subsequent sections.

In the discussion of nonlinear microscopy throughput, the different modalities of nonlinear microscopy can be divided into two subgroups.

Subgroup 1: Modalities that involve nonlinear excitation of molecules to relatively long-lived (i.e., nanoseconds and longer) electronic excited states, and where photonic energy is absorbed by the molecule. This group includes two- and multi-photon fluorescence and phosphorescence excitation processes.

Subgroup 2: Modalities that involve nonlinear excitation of molecules to short-lived (approximately femtoseconds and picoseconds) virtual states or vibronic levels with no effective photonic energy absorption. This group includes modalities such as second- and higher-harmonic generation microscopies and the different nonlinear coherent Raman microscopies.

Almost all NLO microscopy requires raster scanning to obtain volumetric structural information from the specimen; the update rate of the scanner is clearly an important factor in determining imaging speed. However, for the group of modalities with long-lived excited states, the speed of imaging is also partly limited by the excited state lifetime, which determines the maximum rate at which signal photons can be generated per molecule. The rate of signal photon generation determines the minimal residence time required at each raster step to obtain a sufficient signal/noise ratio (SNR) at each image voxel.

The rate of photon-signal generation scales with excitation laser power. Because photonic energy is retained by the excited molecule on the nanosecond timescale, there is a substantial probability that excited-state chemical reactions will occur, resulting in the generation of reactive oxygen species that are the primary factors in causing photobleaching of probe molecules and photodamage to cells and tissues (27). This puts a limit on the maximum power that can be used. Apart from photodamage, excitation saturation often limits the maximum laser power (28). With high peak-power and high repetition-rate pulsed laser sources, a substantial fraction of molecules in the focal volume can be excited, resulting in ground-state depletion for processes with relatively long excited-state lifetimes. With the substantial depletion of the ground state, the probability of NLO interaction has a subquadratic dependence on excitation power, resulting in a degradation of its intrinsic depth-sectioning capability (Fig. 1).

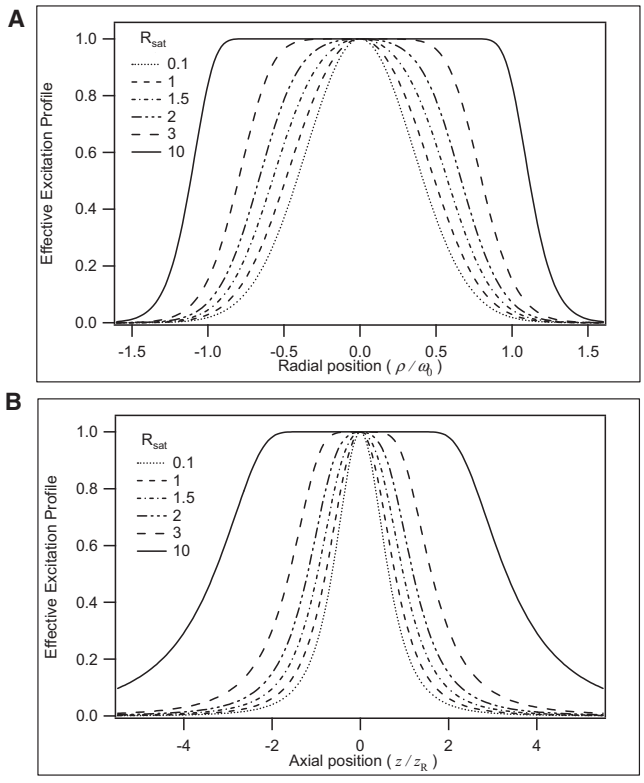

FIGURE 1 Effect of excitation saturation on radial (*top*) and axial (*bottom*) point spread functions at different levels of saturation (28). To see this figure in color, go online.

For the second subgroup of NLO microscopy modalities, the much shorter photointeraction time relaxes many constraints on high-throughput imaging:

The shorter relaxation time can, in principle, result in a significantly higher signal-photon-generation rate, with a corresponding increase in imaging speed; however, this advantage is partly negated by low NLO cross-sections.

Another advantage of this group of NLO modalities is that photobleaching and photodamage by reactive oxygen species is generally not a concern, and higher excitation power may be used; however, the peak power remains limited by damage mechanisms such as dielectric breakdown.

Because the molecular relaxation time is much shorter than the typical maximum laser repetition rate, excitation saturation does not occur due to the cumulative effect of multiple pulses, and higher-throughput imaging can therefore be achieved with higher-repetition-rate lasers.

IMPLEMENTATIONS OF HIGH-THROUGHPUT NONLINEAR OPTICAL MICROSCOPY

Overall, there are two different but complementary approaches to increase the throughput of NLO microscopy. One approach involves increasing the speed of the scanner, reducing the time required at each raster step. The other approach involves parallelizing the imaging process, such that multiple voxels can be imaged at the same time, reducing the number of raster steps needed to cover a three-dimensional volume.

Increased throughput based on improving scanner speed

The idea of improving microscopy throughput by increasing the scanner speed is not new; many of the modalities developed for nonlinear optical microscopes were first developed for confocal microscopy. The adoption of faster scanners for nonlinear microscopes based on their confocal counterparts was fairly straightforward. However, it should be noted that the use of faster scanners provides an advantage only when the signal-photon-generation rate at each voxel is sufficiently high such that the scanners do not need to be slowed down to produce an image with sufficient SNR.

Methods based on high-speed mechanical scanners

Some of the first generation of high-throughput nonlinear optical microscopes replaced slower galvanometric scanners with faster mechanical alternatives, such as polygonal scanners and resonance scanners.

Polygonal scanners consist of a precisely machined cylinder with mirror facets on the perimeter. The rotation of this cylinder is driven by a high-speed motor via an air-bearing. Typical polygonal scanners have several tens of mirror facets and can rotate up to speeds of several tens of thousands of revolutions per minute. The polygonal scanner can thus generate an image at a rate of up to several tens of thousands of scan lines per second. For a moderately-sized image, polygonal scanners readily provide imaging at super-video rate. The first polygonal scanner-based high-throughput nonlinear optical microscope operated in fluorescence mode (29), and was based on a very similarly designed confocal microscope (30). Today, the use of high-speed polygonal scanners has been extended to other nonlinear modalities, including coherent anti-Stokes Raman scattering (31).

The basic design of a polygonal scanner-based nonlinear microscope is shown in Fig. 2. Typically, the polygonal scanner is used only for scanning along one axis. The use of a slower galvanometric scanner is often sufficient for scanning along the orthogonal direction. The lateral position of the focused excitation spot is determined as such. The femtosecond laser light that is incident upon the polygonal scanner is deflected by the scanner and incident upon the mirror of the galvanometric scanner via a 4-F geometry. In this way, the laser spot is stationary on the mirror of the galvanometric scanner. The angular output along one direction is determined by the rotation angle of the polygon, and the other direction by the scan angle of the galvanometer, which is positioned in the eye-point of the scan lens.

Resonance scanners are galvanometric scanners designed to maximize speed. Galvanometric scanners are typically driven under feedback control and can stop at a specific angle accurately, but are relatively slow. However, these scanners can be driven much faster by operating close to their resonance frequency without feedback control. In this mode, the angular position of the mirror is sinusoidal, with a frequency fixed by its mechanical design. The first resonance-scanner-based nonlinear optical microscope was based on a confocal design (32) also operated in fluorescence mode (33), but has subsequently been extended to utilize other contrast mechanisms (34). The integration of

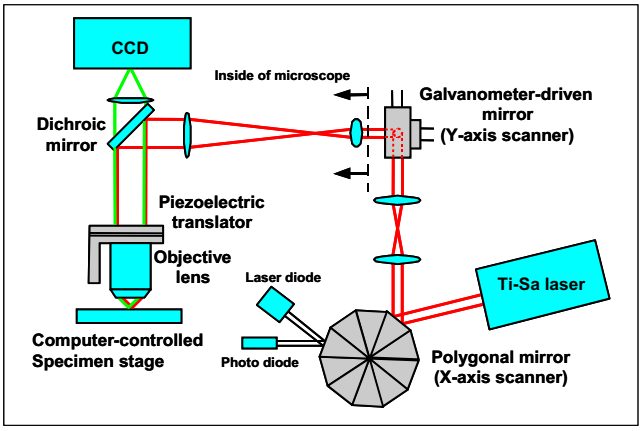

FIGURE 2 Schematics of a polygonal scanner-based NLO microscope (29). The 4-F geometry consists of the optics between the polygonal mirror and the galvanometric mirror. To see this figure in color, go online.

a galvanometric scanner into an NLO microscope involves very similar considerations to the polygonal scanner design and will not be repeated here.

When using polygonal and resonance scanners, it should be noted that neither scanner can be positioned at a specific angle at a given time. Both scanners operate continuously at a constant frequency after some initial warm-up and settling. Therefore, unlike galvanometric scanners, where the scan locations can be set from the instrument control computer synchronizing the whole imaging experiment, the angular positions of these scanners need to be monitored by an independent sensor. As a result, the rest of the instrument (including the galvanometric scanner and the data acquisition module) must be synchronized to these free-running scanners.

Resonance scanners were recently used in the implementation of a stimulated Raman scattering microscope that operated at video rates. Although spontaneous Raman scattering provides excellent chemical specificity, the cross-section of spontaneous Raman scattering is too low for high-throughput imaging. As a coherent process, stimulated Raman scattering (SRS) has a significantly higher cross-section, which allows imaging of a specific vibronic mode with very high efficiency. In addition to improving the scanning speed by utilizing resonance scanning, video-rate imaging based on SRS has overcome many additional technical challenges, including the need to synchronize picosecond lasers providing the pump and the Stokes laser pulses, and the design of a fast lock-in amplifier operating at megahertz frequencies to detect the minute SRS signal within a large Stokes background by operating far from instrument noise interference. The successful implementation of high-throughput SRS microscopy has potential for studying transdermal drug delivery. Preclinical studies on the monitoring of *trans*-retinol acid and DMSO transport through the stratum corneum have been demonstrated (34) (Fig. 3).

Methods based on electro-optical scanners

Another important high-throughput NLO microscope design is based on electro-optical scanners, specifically acousto-optical deflectors (AODs) (35). AODs consist of piezoelectric actuators that are bonded to a crystalline material with high acoustic velocity. Vibration of the piezoactuator sets up a mechanical wave inside the crystal, producing small periodic variations in the mass density and, hence, in the index of refraction. The resulting index of refraction variation acts as a grating and diffracts light traveling through the crystal in accordance with Bragg's Law. The diffraction angle can be readily varied by changing the period of the mechanical vibration within the crystal. In general, the typical AOD access time, and consequently the positional response rate of the device, is approximately tens of microseconds. The access time is limited by the time required for an acoustic wave with a new period to propagate through the crystal.

For a scan line consisting of hundreds to thousands of points, the line-scan rate of AODs is typically comparable to polygonal or resonance mechanical scanners. However, unlike mechanical scanners, which must advance from one location to the next sequentially, the major advantage of an AOD-based NLO microscope is its ability to randomly access different locations near a three-dimensional-resolved plane (35). In many cases, the relevant volume occupied by the specimen of interest is often a very small fraction of an image cube. In monitoring fast kinetic events or minute morphological changes within the specimen of interest, there is little need to acquire data from the whole image cube. In these cases, imaging systems capable of random access offer tremendous throughput advantages. A design for a nonlinear optical microscope with AODs controlling the scanning along both axes is shown in Fig. 4.

Although AOD-based microscopes have unique advantages, they also have specific shortcomings that must be overcome to optimize nonlinear optical imaging. There are two significant complications in using AODs:

First, the crystals used in AODs are typically approximately millimeters to centimeters in length. As a result, femtosecond light pulses, with bandwidths approximately tens of nanometers, will experience group velocity dispersion as they propagate through the AOD crystal. Dispersion results in the broadening of the femtosecond pulse and a reduction in the nonlinear excitation efficiency. This group velocity dispersion can be compensated with dispersion compensators. It should be noted that for very short pulses, higher-order dispersion effects may also be introduced in the long AOD crystals (36–38). In this case, more complex

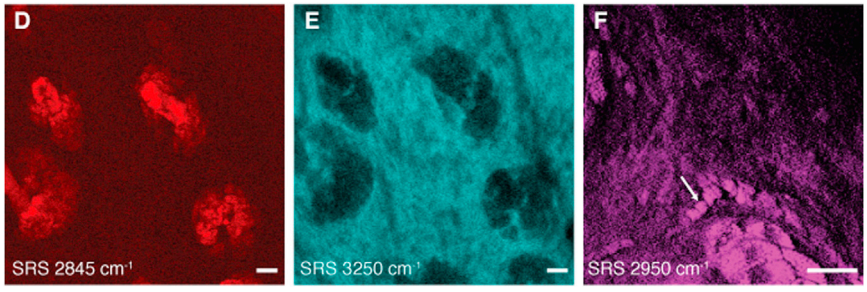

FIGURE 3 *En-face* images of the skin of a live mouse, taken by a video-rate SRS microscope, from reference (34). Images of (D) lipid and (E) water highlight the lipid-rich (but water-poor) sebaceous glands, whereas the CH_3 stretching vibration imaged in (F) serves to highlight proteins and lipid-rich structures. The arrow indicates a capillary in which individual red blood cells can be seen at higher magnification.

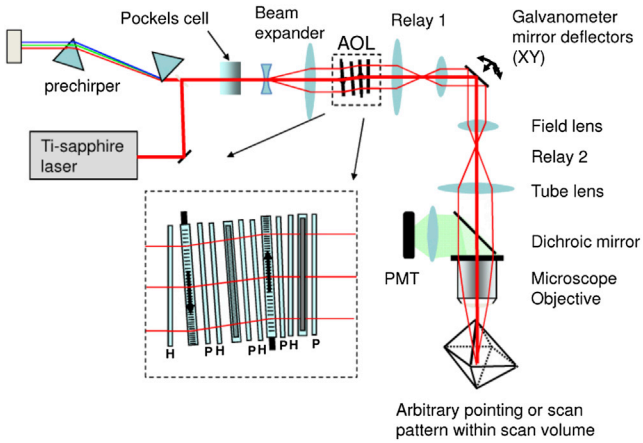

FIGURE 4 A compact AOD-based NLO fluorescence microscope. The prechirper with the paired prism is for temporal dispersion compensation. Acousto-optical lens (AOL) consisting of four AODs (*unlabeled rectangles* with *shaded interior*) with polarizers (*P*) and half-wave plates (*H*) to remove the residue-un-diffracted first-order (70). In this setup, the galvanometer mirrors are fixed and scanning is done solely through the AOL. To see this figure in color, go online.

and expensive higher-order dispersion compensation methods may be required.

Second, AODs also experience chromatic aberrations for ultrashort pulses with large spectral bandwidths. The diffraction angle of an AOD is a function of wavelength and the focus of the diffracted beam is elongated due to the broad spectrum. Several careful designs of AOD-based NLO microscopes seek to remedy this difficulty. One successful design uses a pair of AODs for each scan axis that serves function as a cylindrical lens. The two AODs are arranged such that their chromatic aberrations exactly cancel out for small diffraction angles, although residual chromatic aberrations remain for large diffraction angles. A nice side benefit of this design is that the defocus of these cylindrical lenses can be controlled, allowing axial position control over a small range.

As previously discussed, AOD-based nonlinear microscopes allow random access scanning close to a depth-resolved two-dimensional plane. An important extension of this system is to extend random access scanning to a full three dimensions. In typical raster scanning microscopes, axial scanning is accomplished by translating either the objective or the specimen. In either case, the large mass of the objective limits the mechanical settling time to tens to hundreds of milliseconds. Objective motion at high speed also often mechanically perturbs the specimen. Recently, a remote focusing approach has been developed (39,40). In this technique, the exact optical replica of the specimen is formed at a remote location using an optical train that enables a perfect three-dimensional imaging condition where not only are both sine and Herschel conditions satisfied but also all points near the three-dimensional focal region of the objective are reimaged as points without aberration. The imaging of any plane in the specimen can then be accomplished by positioning a lightweight mirror within this optical replica to project this plane through another microscope system that satisfies the sine condition. High-speed addressing of any axial plane can then be accomplished by rapidly translating the lightweight mirror.

Three-dimensional random access scanning has been applied in the study of signal propagation in neurons in vivo (8). In this implementation, two pairs of AODs provide random addressing in-plane as well as limited axial scanning covering a range of ~60 μm. Pyramidal neurons in the CA1 region of the hippocampus were studied in brain slices in situ. Whole-cell patching was used to introduce a calcium sensor, OGB0-1, and to enable electrical measurement for validation. Based on high-throughput random access imaging, the investigators achieved the monitoring of calcium-signal propagation through different locations along branches of the dendritic tree with millisecond-scale temporal resolution (Fig. 5).

Increase throughput based on parallelized imaging

Increased throughput based on faster scanning is ultimately limited by voxel SNR. Voxel SNR increases with excitation laser power, but is limited by the excited-state lifetime, excitation saturation, and/or specimen damage. Many ultrafast laser sources typically have significantly higher power than is needed for optimizing excitation for a single location. Using these light sources, throughput can be significantly improved by further parallelization, where many locations within the specimen are imaged simultaneously. Several high-throughput NLO microscopes have been designed and implemented with different degrees of parallelization.

Parallelization based on multiple foci excitation

This multifocal multiphoton microscopy approach was first pioneered by Bewersdorf et al. (41), Buist et al. (42), and Kim et al. (43). Instead of focusing the light to a single spot, an array of excitation foci can be produced to parallelize the raster scanning process, to acquire data from several regions in the specimen simultaneously. The advantage of this method is that the imaging speed is enhanced by the degree of parallelization, while mostly maintaining the pixel dwell time and data SNR (41–43). A high-throughput NLO microscope based on the multifocal approach is shown in Fig. 6. A lenslet array (MLA) is used to produce an array of foci from the laser (Ti:Sap) and the beam expander (T). Each excitation beamlet is sent to the objective (OL) via a dichroic mirror (DCM1) and galvanometric scanner (GSM). The galvanometric scanner provides lateral raster scanning, whereas axial translation is achieved with a piezo-positioner (ZP). The specimen is placed on a

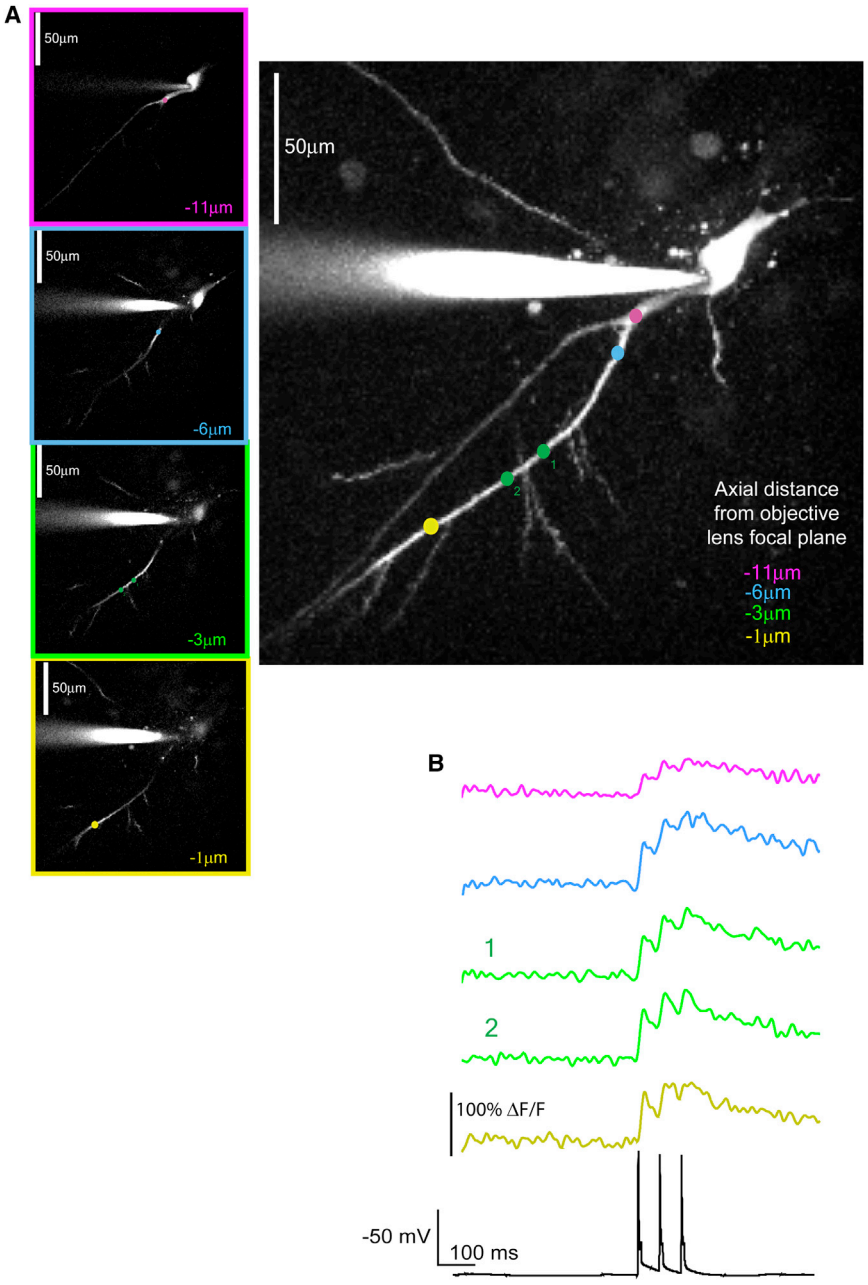

FIGURE 5 (*Top*) An image of calcium-signal propagation along a dendrite of a pyramidal neuron. (*Middle*) The time-dependent calcium signals at selected locations on the dendrite are plotted. (*Bottom*) The neuron is patched to allow simultaneous monitoring of voltage signal (8). To see this figure in color, go online.

three-dimensional translation stage (TS). The signal is detected by a multianode photomultiplier tube (MA-PMT) via a dichroic mirror (DCM2), lens, and a barrier filter (TPB). To overcome the depth-penetration limitation of an NLO microscope in studying very thick specimens, one may integrate an automated, motorized (M), microtome (DH) into the high-throughput NLO microscope system. By alternating and overlapping optical sectioning with mechanical sectioning, it is possible to rapidly image samples of arbitrary thickness.

The multifocal system differs from traditional systems in several ways. An important difference is the need to produce an array of foci in parallel. Many methods have been proposed, including the use of a lenslet array, a beam splitter system (44), an acousto-optical deflector, or a diffractive optical element (45). The lenslet approach was initially used in the designs from Bewersdorf et al. (41) and Buist et al. (42). This approach has been found to be nonoptimal due to uneven power distribution among the foci, resulting from the Gaussian intensity distribution of the excitation laser. Because the imaging speed is limited by the SNR of the focus with the lowest illumination power, it is vital that the available power among the different foci is uniform. The other three approaches all result in significantly more even power distributions. On the other hand, custom beam-splitters suffer from the need to carefully align bulk

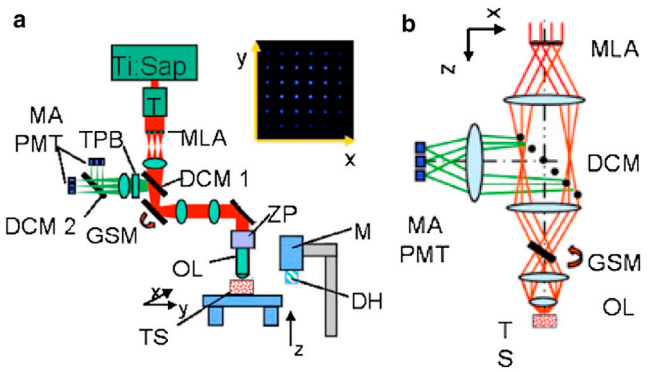

FIGURE 6 Schematic of a multifocal NLO microscope. (*a*) A lenslet array is used to produce an array of foci that are scanned across the sample in a raster pattern. The signal is detected with an MA-PMT. (*Inset*) Fluorescent image of a fluorescein sample excited by the multifocal array. (*b*) An enlarged view of the optical path of the excitation and emission light. (*Ti:Sap*, titanium sapphire laser; *T*, telescope; *MLA*, microlens array; *DCM1*, dichroic mirror 1; *DCM2*, dichroic mirror 2; *GSM*, galvanometric scanning mirror; *MA-PMT*, multianode PMT; *ZP*, z-piezo; *OL*, objective lens; *TS*, tissue sample; *M*, motor; *DH*, microtome; *TPB*, two-photon barrier filter (71).) To see this figure in color, go online.

optics. Acousto-optical deflectors suffer from spectral dispersion and chromatic aberrations, but allow more flexible selection of the number of foci and their separation. Designs with diffractive optical elements require little alignment and are power-efficient, but the number of foci and their separation must be determined a priori, a drawback shared with using lenslet arrays and beam splitters.

Another consideration with the multiple focus design is the optical interference of light between neighboring foci that results in resolution degradation. Several approaches have been implemented to alleviate this problem. Different temporal delays of the femtosecond pulses for each of the different foci may be introduced by inserting an array of optical flats with differing thickness. By temporally separating the pulses, they can no longer interfere with each other (46). However, spatially separating (~100 μm) the foci is also very effective; it is also very simple to implement when using an objective with a large field of view.

One major limitation of the multifocal approach is the significant reduction in imaging depth. A number of recent studies have shown that the high scattering coefficient of tissues poses the most critical impediment for high-resolution deep-tissue imaging (43,47,48). Light is scattered by a combination of Raleigh and Mie mechanisms in tissues. For either mechanism, the cross-section for light scattering decreases with increasing wavelength. The deeper penetration of NLO microscopy relies on the use of infrared excitation that is less attenuated by tissues. However, because the fluorescence or second-harmonic generation emission signal remains in the blue-green spectral range, it suffers significant attenuation from scattering.

As mentioned previously, NLO microscopy provides better deep-tissue imaging capability than techniques such as confocal microscopy because depth selection does not require the presence of a pinhole aperture in the emission light path. Unfortunately, because a multifocal NLO microscope typically uses an imaging camera as its detector, each individual pixel of the camera behaves as a pinhole aperture. Scattered emission photons do not arrive in the appropriate pixel but distribute into the background of the image, with the result that the typical multifocal multiphoton microscopy approach is incapable of deep-tissue imaging. To overcome this problem, recent work has quantified the effect of scattering of emission photons on image resolution and contrast (43).

It was found that scattering primarily acts to reduce image contrast but weakly affects image resolution. Based on this understanding of tissue optics, a multifocal NLO microscope has been implemented using a multianode photomultiplier tube (MA-PMT) that is capable of high-speed imaging in deep tissues (43,49), with performance comparable to traditional two-photon microscopes. The use of an MA-PMT mostly overcomes the problem with the scattered emission photons. Because the MA-PMT is placed at the image plane after descanning, each anode effectively covers a large spatial region corresponding to the foci separation (~100 μm). The large effective area allows much more effective collection of the scattered emission photons by each anode. Importantly, there will still be scattered emission photons leaking to adjacent anodes resulting in some degree of cross-talk. Work has shown that these scattered emission photons can be effectively reassigned to the correct location based on maximum likelihood algorithms.

Recently, another approach has been developed that simultaneously overcomes the issue of multiple foci generation and optimization of the collection of scattered emission photons. In this approach, a custom-designed optical multiplexer generates several temporally interlaced pulse trains (with temporal separation of several nanoseconds) that can be focused at different locations or depths (50,51). These multiple beams are then raster-scanned across the image. Because the beams are separated in time (which provides temporal encoding of the excitation position), the almost simultaneously-generated signals from multiple spatial locations can be distinguished using high-speed electronics.

The advantage of this method lies in eliminating the need for an image sensor, with the associated SNR loss due to the scattering of emission photons. However, a limitation of this method lies in the fact that the degree of parallelization is relatively limited. The fluorophore lifetime sets the minimum time separation and the pulse separation of the laser sets the total time duration within which pulses can be multiplexed. This system has been applied to monitor calcium-signal propagation in neurons (52). In an in vivo mouse model, four beams were multiplexed to simultaneously image two depths, where each layer is covered by two of the beams to increase throughput. The investigators

successfully showed that calcium transients of these neurons can be monitored with a temporal resolution of ~4 ms. This study demonstrates the potential for monitoring communications between a population of neurons from different layers in the cortex (Fig. 7).

Parallelization based on temporal focusing wide-field excitation

As discussed, multifocal excitation is a successful parallelization approach. Temporal focusing multiphoton microscopy can be considered as a method with an even higher degree of parallelization (by a factor of 10^2–10^4) (53–55). Fig. 8 demonstrates the underlying concepts behind spatial focusing and temporal focusing. In Fig. 8 *a* (*left*), an optical pulse is focused laterally in the spatial dimension, traveling along the axial direction. Note that its temporal pulse width is kept constant. The intensity at the focal spot reaches a maximum. Nonlinear optical processes such as two-photon absorption are proportional to the square of the pulse peak power, which results in optical sectioning. For a high numerical-aperture objective, submicron lateral and axial resolution can be achieved. With temporal focusing, the optical pulse travels in the axial direction without changing the beam diameter, unlike spatial focusing (Fig. 8 *a*, *right*). However, the instantaneous intensity will be maximized at the focal plane, if the temporal width of the optical pulse can be manipulated spatially, such that it is minimized at the focal plane.

This approach allows wide-field imaging with depth discrimination. The trick to generate temporal focusing is to control the temporal width of ultrafast pulses. The temporal width (τ) of an ultrafast pulse is related to its spectral bandwidth ($\Delta\lambda$); the time-bandwidth product ($\tau\Delta\lambda$) is a constant for transform-limited pulses. Therefore, the generation of broadened pulses can be accomplished by spectrally limiting their bandwidths. A very simple geometry to accomplish this task has been proposed by Oron et al. (53) (Fig. 8 *b*). The temporal focusing principle can be realized in a 4-F geometry by introducing a dispersive element, such as a diffraction grating, to the back focal plane of the tube lens, sending different spectral components of an optical pulse in different directions (different incident angles relative to the optical axis). For an aberration-free system (including chromatic aberration), these different spectral components have the same path lengths to the objective

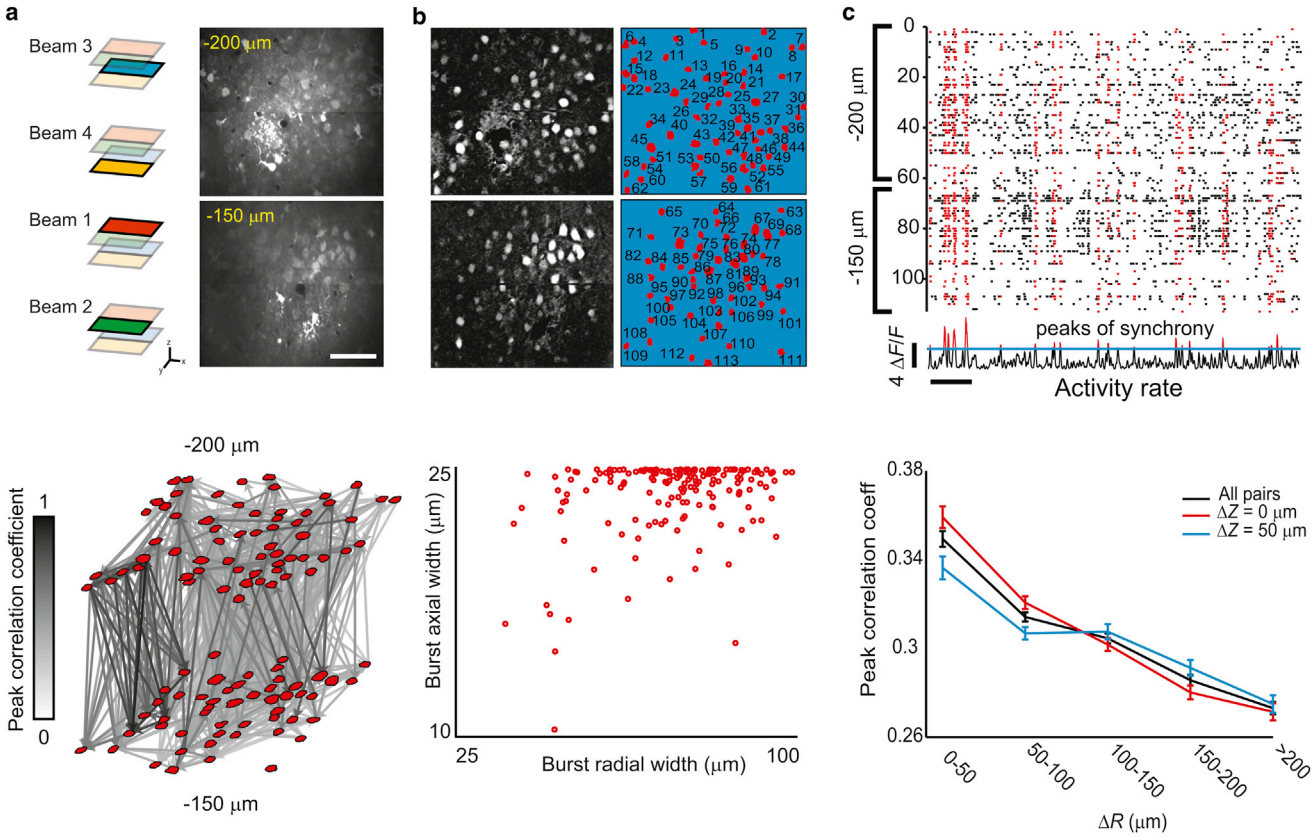

FIGURE 7 (*a*) Scan patterns used with a four-beam multifocal NLO microscope, with representative images of calcium signals, using Fluo-4-AM, from neurons imaged at two levels in the brain. (*b*) Zero time-lag calcium-signal images of neurons taken at two depths (*left*) and the corresponding segmented image (*right*). (*c*) Raster plot showing firing events from labeled cells identified at the two layers (*y* axis) as a function of time (*x* axis). (*Red dots*) Synchronous correlated firing event; (*black dots*) firings that are not well correlated. A representative firing pattern for two cells is shown below the raster plot, containing both correlated and uncorrelated events (52). To see this figure in color, go online.

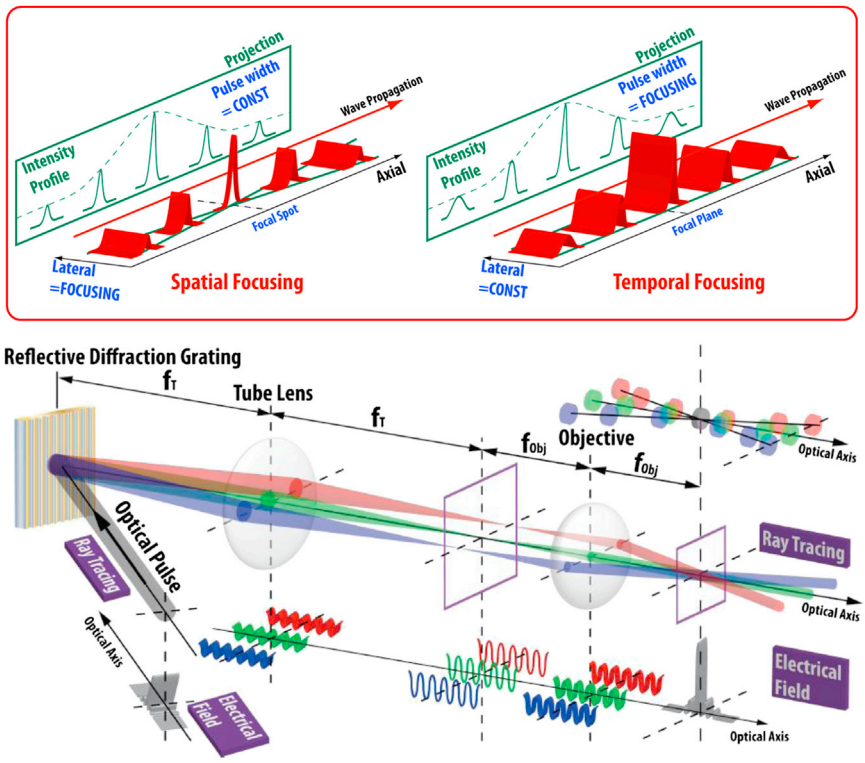

FIGURE 8 (*a*) Principles of spatial and temporal focusing NLO microscopy. (*b*) Schematics of a temporal-focusing NLO microscope based on the design by Oron et al. (53). To see this figure in color, go online.

front focal plane where they recombine. When all the wavelength components recombine, the ultrafast pulses retain their narrow femtosecond pulse width. For the 4-F system, this path-length-matching property is true only at the back focal plane of the tube lens and the front focal plane of the objective, but not anywhere else. Therefore, outside the focal plane, the path lengths for the different spectral components are different; the pulses broaden, and the excitation efficiency decreases.

Although temporal-focusing-based imaging was invented several years ago, its level of adoption in the field is limited by several technical difficulties, including its limited axial resolution, low-excitation efficiency, unrealized frame rate, and its more limited tissue-penetration depth. As innovative researchers start focusing on this area, one may expect that many of these difficulties will be overcome. For example, recent work by Vaziri and Shank (56) demonstrated that temporal-focusing wide-field imaging with axial resolution can be comparable to the single-focus approach if the spectral components of the laser pulse are better distributed at the back aperture of the objective. Another very interesting piece of recent work has shown that temporal focusing is less sensitive to the influence of tissue scattering, and may provide improved imaging depth (57,58). The need for high peak power to achieve effective temporal-focusing wide-field excitation has recently been partly overcome by using regenerative amplifiers as laser sources (59), as well as the use of high NLO cross-section probes (60). Importantly, the relative immaturity of this area offers ample opportunities for innovations, including interesting work in optogenetic control (61), superresolution imaging (62), and high-throughput three-dimensional microfabrication (63).

One application of wide-field temporal-focusing excitation for high-throughput imaging is in the area of fluorescence (FLIM) and phosphorescence (PLIM) lifetime microscopy. FLIM and PLIM are important modalities for studying protein interactions via resonance energy transfer, and for monitoring oxygen concentration via quenching mechanisms. Accurate spectroscopic measurements require high SNR, resulting in a long voxel residence time. The situation is particularly challenging for phosphorescence measurement, where imaging speed is limited by the long phosphorescence lifetime of probes, which can be on the order of milliseconds, resulting in three-dimensional imaging with exceptionally slow-image frame rate. This difficulty has recently been overcome by combining temporal-focusing wide-field imaging for three-dimensionally resolved excitation over a whole plane with frequency-domain heterodyne wide-field imaging (60). This approach has resulted in fluorescence wide-field imaging with integration times per frame as low as several milliseconds, and allows three-dimensional mapping of oxygen distribution in tissue regeneration constructs (Fig. 9) (60).

CONCLUSION

Over the past decade, very exciting technical developments in high-throughput NLO microscopy based on increasing

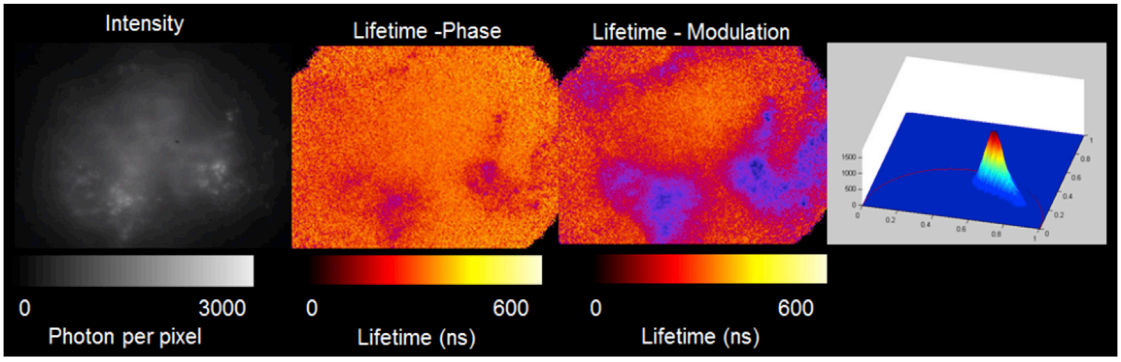

FIGURE 9 Fast three-dimensionally resolved temporal-focusing wide-field FLIM-PLIM imaging of a sample consisting of human fibroblasts stained with Rhodamine lipid, seeded inside a collagen matrix and treated in buffer containing 1 mM ruthenium-based oxygen sensor. (In sequence from *left* to *right*) Intensity image, phosphorescence lifetime-resolved image from phase data, and phosphorescence lifetime-resolved image from modulation data. (*Far right*) Polar plot of the pixel phosphorescence lifetime-resolved measurements (60). To see this figure in color, go online.

scanning speed and/or increasing the degree of parallelization have been developed. These techniques improve imaging speed to different degrees, and their implementations often involve accepting tradeoffs in performance characteristics such as SNR, image resolution, implementation simplicity, and instrument cost. As these technologies become more mature, it is expected that these different modalities of high-throughput NLO microscopy will find their niches within different biological and medical applications. The development of increasingly-sensitive detectors will help increase throughput, but are beyond the scope of this review.

Looking forward into the future, it may be interesting to speculate as to future technologies that may be used to further enhance the performance of high-throughput NLO microscopy. One promising approach is the adaptation of serial time-encoded amplified microscopy (STEAM) (64) for NLO imaging. STEAM has been developed for image cytometry with contrast based on linear scattering and absorption of light. In STEAM, an ultrafast laser pulse is dispersed over the surface of interest, such that each location is encoded using a different wavelength component of the pulse (see Fig. 10 and Table 1). Light scattered from each point is coupled into a single highly-dispersive optical fiber. The optical dispersion causes the pulse to spread out in time, so the intensity at each wavelength, and hence each location, can be measured using a high-speed photodiode, eliminating the need for image sensor arrays that often have comparatively low readout rates, and offering the possibility of signal amplification using integrated fiber amplifiers. Image cytometry with an impressive subnanosecond shutter speed has been achieved (65).

We foresee that this approach may be applicable for NLO imaging especially for coherent techniques using

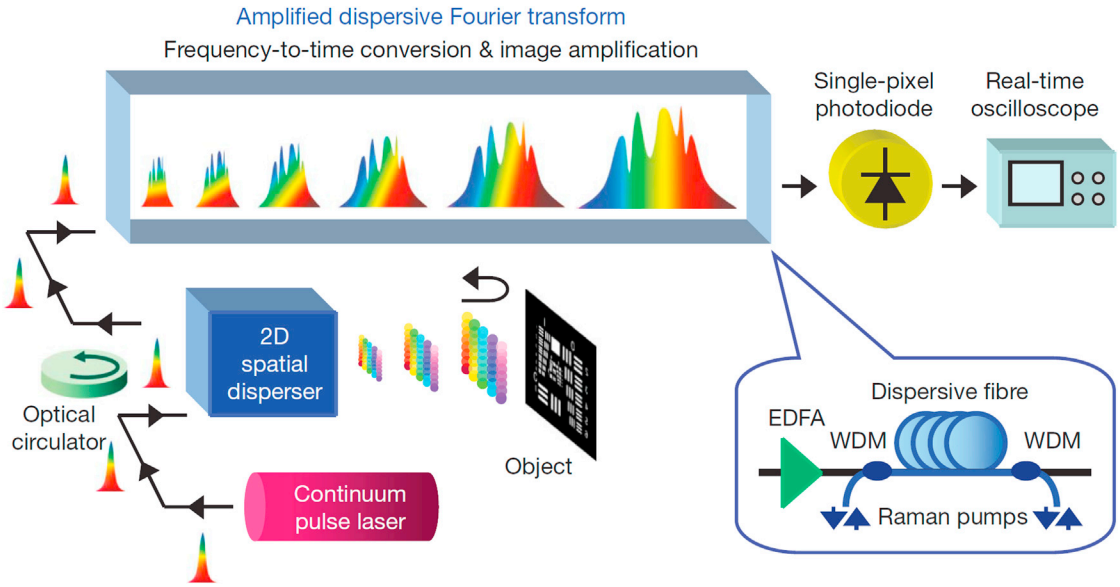

FIGURE 10 Schematics of a STEAM white light image cytometer. (3). To see this figure in color, go online.

TABLE 1 Pros and Cons of various high-throughput imaging modalities

Function	Technology	Pros	Cons	References
Polygonal mirrors	Cylinder is machined to have many facets that reflect light when spun at high speeds.	>10,000 scan lines/s. Progression of scan is necessarily sequential.	User unable to determine where to point the scanner. Requires separate sensing device. Microscope must be synchronized to the scanner.	(2,38)
Resonance scanners	Standard galvanometric mirror that is operated at resonance frequency and without feedback.	Faster than galvanometric scanners. Essentially galvanometric scanner without feedback. Operates at a constant frequency after settling.	User unable to determine where to point the scanner. Requires separate sensing device. Microscope must be synchronized to the scanner.	(1)
Acousto-optic deflector	Grating induced in the crystal through an applied mechanical wave that causes a change in refractive index. Angular deviation of light is determined by the frequency of mechanical wave.	Fast response (tens of microseconds). Arbitrary/random access of sample. Speed comparable to resonance or polygonal scanners in some instances. Possible to also do axial scanning to a slight degree.	Dispersion leading to broader pulse. Requires precompensation device. Chromatic aberrations, especially for short pulses or large diffraction angles.	(7)
Remote focusing	Forms an exact replica of the object optically. This replica satisfies the sine and Herschel condition. Axial scanning is achieved by scanning a lightweight mirror within this replica.	Much faster than scanning the objective. Imaging is theoretically correct because both sine and Herschel conditions are satisfied. Object is not perturbed in any way.	Requires careful matching of optics and objectives. Requires a relaying microscope setup to relay the scanned replicated image.	(45,46)
Multiple foci	Splits the excitation light beam into multiple beams that each form their own focus on the object. Uses beamsplitters, lenslet arrays, acousto-optic deflectors, or diffractive optical elements.	Data extracted from multiple regions simultaneously. Dwell time and signal/noise preserved. Possible for configuring beamlets on-the-fly when using acousto-optical deflectors. Spatial or temporal separation and use of multianode photomultiplier tubes can help reduce scattering and increase imaging depth.	Critical to maintain evenness of illumination over all beamlets. May suffer from inefficient use of excitation beam. May require careful alignment. Poor imaging depth achieved due to scattering (but addressable).	(9,49,55–57)
Temporal focusing	Based on the time-bandwidth product. Input pulsed beam is focused in time instead of space. Spatial dimensions are thus preserved, making the system wide-field but with optical sectioning.	Wide-field excitation. Optical sectioning due to the two-photon absorption. Possible to achieve submicron axial resolution. Very high frame rates. Excitation is less sensitive to tissue scattering. Axial scanning through optical means.	Imaging depth still limited by scattering of signal. Relatively poor axial resolution, unless a more complex setup is used. Low excitation efficiency.	(6,58,60–66)

picosecond pulses, such as stimulated Raman imaging, where broad bandwidth lasers can be multiplexed into tens of locations based on spectral separation. By synchronizing two ultrafast pulses (pump and Stokes) differing in energy by the energy of a vibrational transition in an analyte of interest, chemoselective imaging can be performed. The pump beam can be modulated at several megahertz, and the Stokes beam measured using lock-in detection at the modulation frequency. In this manner, it should be possible to obtain single-shot chemoselective images, with a frame-rate controlled by the repetition rate of the laser and resolution controlled by the achievable spatial dispersion, permitting much higher resolution images at faster frame-rates than are possible using raster scanning.

Another direction for further development may lie in further parallelization. While temporal focusing allows simultaneous whole-plane imaging, the construction of a three-dimensional image cube still requires axial scanning. It is known that in the temporal focusing approach, the plane of excitation can be shifted axially by introducing a quadratic spectral chirp to the excitation pulse, which can be considered as the temporal analog of a spatial defocus (55,66). The plane of excitation can be positioned above or below the normal focal plane of the objective up to a range of ~100 μm, offering the possibility of carrying out simultaneous volumetric imaging. For a broad-spectrum ultrafast pulse, multiple beams that are spectrally separated can be chirped with different quadratic parameters so as to focus at different depths. The signal from multiple z planes can be imaged simultaneously onto a detector. The drawback of such an approach is that there will only be one plane that is in focus at the detector and the result is an image that is no better than that captured with conventional wide-field microscopy.

To bring all the different planes into focus, it is necessary to correct for the defocus. This may be done either by using a cubic phase mask (67) or with a volume hologram. The first method (cubic phase mask) requires an additional post-processing step of deconvolving the captured image with the point-spread function (68); the deconvolved image is therefore equivalent to the sum of all the planes. The second method (volume hologram) is based on using a multiplexed holographic Bragg filter, which compensates for the defocus while mapping axial depths to a transverse shift on the detector (69).

In summary, many of these NLO microscopes enable high-throughput imaging of morphological information in three dimensions, but provide relatively limited spectroscopic information. Although morphological information is always important, an important strength of microscopy with NLO contrast is the rich spectroscopic content available for elucidating complex cell- and tissue-biochemical processes. As examples, hyperspectral imaging performed to resolve multiple endogenous fluorophores based on their unique emission spectrum has been shown to provide important diagnostic information in different diseases. Spectrally resolved coherent Raman spectroscopy will allow the monitoring of multiple chemical species. Fluorescence lifetime-resolved imaging of resonance energy transfer between protein species should enable the study of protein signaling in vivo. And, finally, polarization-resolved imaging of harmonic signals may provide important clues related to the conformation of macromolecules. Common to all these spectroscopic applications is the ability to quantify the wavelength, phase, and polarization of light at high throughput. The development of high-throughput spectroscopy coupled with NLO microscopy should be a very rich area of research in the future.

PTCS acknowledges support from: NIH 9P41EB015871-26A1, R01-EX017656, 5 R01 NS051320, 4R44EB012415-02, NSF CBET-0939511, the Singapore-MIT Alliance 2, and the MIT SkolTech initiative. EYYS is supported by the National Research Foundation Singapore through the Singapore MIT Alliance for Research and Technology's BioSym research programme. CJR is funded by a Wellcome Trust MIT Postdoctoral Research Fellowship 093831/Z/10/Z.

REFERENCES

1. Göppert-Mayer, M. 1931. Regarding elementary acts with two quantum jumps [Über elementarakte mit zwei quantensprüngen]. *Ann. Phys.* (*Leipzig*). 5:273–294.
2. Sheppard, C. J. R., J. N. Gannaway, …, D. Walsh. 1977. Scanning harmonic optical microscope. *IEEE J. Quantum Electron.* 13:D100.
3. Denk, W., J. H. Strickler, and W. W. Webb. 1990. Two-photon laser scanning fluorescence microscopy. *Science.* 248:73–76.
4. Masters, B. R., and P. T. C. So, editors. 2008. Handbook of Biomedical Non-Linear Optical Microscopy Oxford University Press, New York.
5. So, P. T., C. Y. Dong, …, K. M. Berland. 2000. Two-photon excitation fluorescence microscopy. *Annu. Rev. Biomed. Eng.* 2:399–429.
6. Min, W., C. W. Freudiger, …, X. S. Xie. 2011. Coherent nonlinear optical imaging: beyond fluorescence microscopy. *Annu. Rev. Phys. Chem.* 62:507–530.
7. Sacconi, L., C. Ferrantini, …, F. S. Pavone. 2012. Action potential propagation in transverse-axial tubular system is impaired in heart failure. *Proc. Natl. Acad. Sci. USA.* 109:5815–5819.
8. Duemani Reddy, G., K. Kelleher, …, P. Saggau. 2008. Three-dimensional random access multiphoton microscopy for functional imaging of neuronal activity. *Nat. Neurosci.* 11:713–720.
9. Lee, S., C. Vinegoni, …, R. Weissleder. 2012. Real-time in vivo imaging of the beating mouse heart at microscopic resolution. *Nat. Commun.* 3:1054.
10. Dimitrow, E., M. Ziemer, …, M. Kaatz. 2009. Sensitivity and specificity of multiphoton laser tomography for in vivo and ex vivo diagnosis of malignant melanoma. *J. Invest. Dermatol.* 129:1752–1758.
11. Patalay, R., C. Talbot, …, C. Dunsby. 2012. Multiphoton multispectral fluorescence lifetime tomography for the evaluation of basal cell carcinomas. *PLoS ONE.* 7:e43460.
12. He, Y., C. H. Kang, …, H. Yu. 2010. Towards surface quantification of liver fibrosis progression. *J. Biomed. Opt.* 15:056007.
13. Tai, D. C., N. Tan, …, H. Yu. 2009. Fibro-C-Index: comprehensive, morphology-based quantification of liver fibrosis using second harmonic generation and two-photon microscopy. *J. Biomed. Opt.* 14:044013.
14. Bélanger, E., S. Bégin, …, D. Côté. 2009. Quantitative myelin imaging with coherent anti-Stokes Raman scattering microscopy: alleviating the

excitation polarization dependence with circularly polarized laser beams. *Opt. Express.* 17:18419–18432.

15. Huff, T. B., Y. Shi, …, J. X. Cheng. 2011. Real-time CARS imaging reveals a calpain-dependent pathway for paranodal myelin retraction during high-frequency stimulation. *PLoS ONE.* 6:e17176.
16. Perlman, Z. E., T. J. Mitchison, and T. U. Mayer. 2005. High-content screening and profiling of drug activity in an automated centrosome-duplication assay. *ChemBioChem.* 6:145–151.
17. Perlman, Z. E., M. D. Slack, …, S. J. Altschuler. 2004. Multi-dimensional drug profiling by automated microscopy. *Science.* 306:1194–1198.
18. Yarrow, J. C., G. Totsukawa, …, T. J. Mitchison. 2005. Screening for cell migration inhibitors via automated microscopy reveals a Rho-kinase inhibitor. *Chem. Biol.* 12:385–395.
19. Eggert, U. S., A. A. Kiger, …, C. M. Field. 2004. Parallel chemical genetic and genome-wide RNA$_i$ screens identify cytokinesis inhibitors and targets. *PLoS Biol.* 2:e379.
20. Kau, T. R., F. Schroeder, …, P. A. Silver. 2003. A chemical genetic screen identifies inhibitors of regulated nuclear export of a Forkhead transcription factor in PTEN-deficient tumor cells. *Cancer Cell.* 4:463–476.
21. Wignall, S. M., N. S. Gray, …, R. Heald. 2004. Identification of a novel protein regulating microtubule stability through a chemical approach. *Chem. Biol.* 11:135–146.
22. Snyder, J. R., A. Hall, …, S. J. Orlow. 2005. Dissection of melanogenesis with small molecules identifies prohibitin as a regulator. *Chem. Biol.* 12:477–484.
23. Corcoran, L. J., T. J. Mitchison, and Q. Liu. 2004. A novel action of histone deacetylase inhibitors in a protein aggresome disease model. *Curr. Biol.* 14:488–492.
24. Pelish, H. E., J. R. Peterson, …, T. Kirchhausen. 2006. Secramine inhibits Cdc42-dependent functions in cells and Cdc42 activation in vitro. *Nat. Chem. Biol.* 2:39–46.
25. Lang, P., K. Yeow, …, A. Scheer. 2006. Cellular imaging in drug discovery. *Nat. Rev. Drug Discov.* 5:343–356.
26. Loo, L. H., L. F. Wu, and S. J. Altschuler. 2007. Image-based multivariate profiling of drug responses from single cells. *Nat. Methods.* 4:445–453.
27. König, K., P. T. So, …, E. Gratton. 1997. Cellular response to near-infrared femtosecond laser pulses in two-photon microscopes. *Opt. Lett.* 22:135–136.
28. Nagy, A., J. Wu, and K. M. Berland. 2005. Observation volumes and γ-factors in two-photon fluorescence fluctuation spectroscopy. *Biophys. J.* 89:2077–2090.
29. Kim, K. H., C. Buehler, and P. T. C. So. 1999. High-speed, two-photon scanning microscope. *Appl. Opt.* 38:6004–6009.
30. Rajadhyaksha, M., M. Grossman, …, R. R. Anderson. 1995. In vivo confocal scanning laser microscopy of human skin: melanin provides strong contrast. *J. Invest. Dermatol.* 104:946–952.
31. Evans, C. L., E. O. Potma, …, X. S. Xie. 2005. Chemical imaging of tissue in vivo with video-rate coherent anti-Stokes Raman scattering microscopy. *Proc. Natl. Acad. Sci. USA.* 102:16807–16812.
32. Tsien, R. Y., and B. J. Bacskai. 1995. Video-rate confocal microscopy. *In* Handbook of Biological Confocal Microscopy. J. B. Pawley, editor. Plenum Press, New York, pp. 459–478.
33. Fan, G. Y., H. Fujisaki, …, M. H. Ellisman. 1999. Video-rate scanning two-photon excitation fluorescence microscopy and ratio imaging with chameleons. *Biophys. J.* 76:2412–2420.
34. Saar, B. G., C. W. Freudiger, …, X. S. Xie. 2010. Video-rate molecular imaging in vivo with stimulated Raman scattering. *Science.* 330:1368–1370.
35. Iyer, V., T. M. Hoogland, and P. Saggau. 2006. Fast functional imaging of single neurons using random-access multiphoton (RAMP) microscopy. *J. Neurophysiol.* 95:535–545.
36. Xi, P., Y. Andegeko, …, M. Dantus. 2009. Two-photon imaging using adaptive phase compensated ultrashort laser pulses. *J. Biomed. Opt.* 14:014002.
37. Iyer, V., B. E. Losavio, and P. Saggau. 2003. Compensation of spatial and temporal dispersion for acousto-optic multiphoton laser-scanning microscopy. *J. Biomed. Opt.* 8:460–471.
38. Reddy, G. D., and P. Saggau. 2005. Fast three-dimensional laser scanning scheme using acousto-optic deflectors. *J. Biomed. Opt.* 10:064038.
39. Botcherby, E. J., C. W. Smith, …, T. Wilson. 2012. Aberration-free three-dimensional multiphoton imaging of neuronal activity at kHz rates. *Proc. Natl. Acad. Sci. USA.* 109:2919–2924.
40. Botcherby, E. J., R. Juskaitis, …, T. Wilson. 2008. An optical technique for remote focusing in microscopy. *Opt. Commun.* 281:880–887.
41. Bewersdorf, J., R. Pick, and S. W. Hell. 1998. Multifocal multiphoton microscopy. *Opt. Lett.* 23:655–657.
42. Buist, A. H., M. Muller, …, G. J. Brakenhoff. 1998. Real time two-photon absorption microscopy using multipoint excitation. *J. Microsc.* 192:217–226.
43. Kim, K. H., C. Buehler, …, P. T. So. 2007. Multifocal multiphoton microscopy based on multianode photomultiplier tubes. *Opt. Express.* 15:11658–11678.
44. Nielsen, T., M. Fricke, …, P. Andresen. 2001. High efficiency beam splitter for multifocal multiphoton microscopy. *J. Microsc.* 201:368–376.
45. Sacconi, L., E. Froner, …, F. S. Pavone. 2003. Multiphoton multifocal microscopy exploiting a diffractive optical element. *Opt. Lett.* 28:1918–1920.
46. Andresen, V., A. Egner, and S. W. Hell. 2001. Time-multiplexed multifocal multiphoton microscope. *Opt. Lett.* 26:75–77.
47. Dong, C. Y., K. Koenig, and P. So. 2003. Characterizing point spread functions of two-photon fluorescence microscopy in turbid medium. *J. Biomed. Opt.* 8:450–459.
48. Dong, C. Y., B. Yu, …, P. T. So. 2004. Performances of high numerical aperture water and oil immersion objective in deep-tissue, multi-photon microscopic imaging of excised human skin. *Microsc. Res. Tech.* 63:81–86.
49. Bahlmann, K., P. T. So, …, K. Bellve. 2007. Multifocal multiphoton microscopy (MMM) at a frame rate beyond 600 Hz. *Opt. Express.* 15:10991–10998.
50. Carriles, R., K. E. Sheetz, …, V. Barzda. 2008. Simultaneous multi-focal, multiphoton, photon counting microscopy. *Opt. Express.* 16:10364–10371.
51. Amir, W., R. Carriles, …, J. A. Squier. 2007. Simultaneous imaging of multiple focal planes using a two-photon scanning microscope. *Opt. Lett.* 32:1731–1733.
52. Cheng, A., J. T. Gonçalves, …, C. Portera-Cailliau. 2011. Simultaneous two-photon calcium imaging at different depths with spatiotemporal multiplexing. *Nat. Methods.* 8:139–142.
53. Oron, D., E. Tal, and Y. Silberberg. 2005. Scanningless depth-resolved microscopy. *Opt. Express.* 13:1468–1476.
54. Tal, E., D. Oron, and Y. Silberberg. 2005. Improved depth resolution in video-rate line-scanning multiphoton microscopy using temporal focusing. *Opt. Lett.* 30:1686–1688.
55. Durst, M. E., G. Zhu, and C. Xu. 2006. Simultaneous spatial and temporal focusing for axial scanning. *Opt. Express.* 14:12243–12254.
56. Vaziri, A., and C. V. Shank. 2010. Ultrafast widefield optical sectioning microscopy by multifocal temporal focusing. *Opt. Express.* 18:19645–19655.
57. Dana, H., N. Kruger, …, S. Shoham. 2013. Line temporal focusing characteristics in transparent and scattering media. *Opt. Express.* 21:5677–5687.
58. Dana, H., and S. Shoham. 2011. Numerical evaluation of temporal focusing characteristics in transparent and scattering media. *Opt. Express.* 19:4937–4948.

59. Cheng, L. C., C. Y. Chang, …, S. J. Chen. 2012. Spatiotemporal focusing-based widefield multiphoton microscopy for fast optical sectioning. *Opt. Express.* 20:8939–8948.

60. Choi, H., D. S. Tzeranis, …, P. T. So. 2012. 3D-resolved fluorescence and phosphorescence lifetime imaging using temporal focusing wide-field two-photon excitation. *Opt. Express.* 20:26219–26235.

61. Andrasfalvy, B. K., B. V. Zemelman, …, A. Vaziri. 2010. Two-photon single-cell optogenetic control of neuronal activity by sculpted light. *Proc. Natl. Acad. Sci. USA.* 107:11981–11986.

62. Vaziri, A., J. Tang, …, C. V. Shank. 2008. Multilayer three-dimensional super resolution imaging of thick biological samples. *Proc. Natl. Acad. Sci. USA.* 105:20221–20226.

63. Kim, D., and P. T. So. 2010. High-throughput three-dimensional lithographic microfabrication. *Opt. Lett.* 35:1602–1604.

64. Goda, K., K. K. Tsia, and B. Jalali. 2009. Serial time-encoded amplified imaging for real-time observation of fast dynamic phenomena. *Nature.* 458:1145–1149.

65. Goda, K., A. Ayazi, …, B. Jalali. 2012. High-throughput single-microparticle imaging flow analyzer. *Proc. Natl. Acad. Sci. USA.* 109:11630–11635.

66. Suchowski, H., D. Oron, and Y. Silberberg. 2006. Generation of a dark nonlinear focus by spatio-temporal coherent control. *Opt. Commun.* 264:482–487.

67. Somayaji, M., V. R. Bhakta, and M. P. Christensen. 2012. Experimental evidence of the theoretical spatial frequency response of cubic phase mask wavefront coding imaging systems. *Opt. Express.* 20:1878–1895.

68. Dowski, Jr., E. R., and W. T. Cathey. 1995. Extended depth of field through wave-front coding. *Appl. Opt.* 34:1859–1866.

69. Liu, W., D. Psaltis, and G. Barbastathis. 2002. Real-time spectral imaging in three spatial dimensions. *Opt. Lett.* 27:854–856.

70. Kirkby, P. A., K. M. Srinivas Nadella, and R. A. Silver. 2010. A compact acousto-optic lens for 2D and 3D femtosecond based 2-photon microscopy. *Opt. Express.* 18:13721–13745.

71. Ragan, T., J. D. Sylvan, …, P. T. So. 2007. High-resolution whole organ imaging using two-photon tissue cytometry. *J. Biomed. Opt.* 12:014015.